Effect of Scanning Speed and Powder Flow Rate on the Evolving Properties of Laser Metal Deposited Ti-6Al-4V/Cu Composites

Mutiu F. **Erinosho**[1,*], Esther T. **Akinlabi**[1], Sisa **Pityana**[2]

[1]Department of Mechanical Engineering Science, University of Johannesburg, Auckland Park Kingsway Campus, Johannesburg, South Africa, 2006.

[2] National Laser Centre, Council for Scientific and Industrial Research (CSIR), Pretoria 0001, South Africa.

*Corresponding author: mutiuerinosho@yahoo.com

Abstract

In Laser Metal Deposition (LMD), good bonding between two similar or dissimilar materials can be achieved if the interrelationships between the processing parameters are well understood. LMD samples of titanium alloy, Ti-6Al-4V and copper, Cu were produced by varying the scanning speed and keeping other parameters constant. The deposited samples were characterized through the volume of deposited composites, microstructure, microhardness and the degree of porosity. The effect of the optimized high (powder flow rate) PFR, scanning speed varying from 0.06 m/min to 1.2 m/min and a constant power of 1kW led to a degree of porosity on the deposited composites. The varying percentages of porosities in the samples have an advance merit effect in the implantation of bones in animal and human. It was found that the existence of pores reduced as the scanning speed increases. The Vickers mirohardness was observed to increase with an increase in the scanning speed which shows an improvement in the properties of the Ti-6Al-4V/Cu composites. At low scanning velocity, the microstructure appears coarse due to the high rate of powder deposited at the same power of 1kW. The α-phase acicular microstructure decreases in size and thickness with an increase in the scanning speed. Widmanstätten structure was found in the

scanning electron microscopy analyses. The results show that high PFR and low scanning speed have significantly influenced the evolving properties of the deposited composites.

Key words: *Hardness, high PFR, laser metal deposition, microstructure, porosity, and volume of deposited composite*

1. INTRODUCTION

Titanium has been known for years back and has improved the efficiency and functionality of some niche components in the industry today. The laser technology process is very vital in all walks of life since it can travel a wide range of distance and can be focused to a small bright spot that exceed that of the sun. Additive manufacturing (AM) has proved a greater effectiveness from the production stage to the final successful finished layer with the aid of the CAD software tool technology (Wohlers, 2011). It is highly in demand in the aerospace, marine industrial, bio-medicals, chemical, and automotive industrial services due to the combination of properties (Moiseyev, 2006; Lutjering and Williams, 2007). According to the (Common Materials, accessed in 2014), Ti-6Al-4V is significantly stronger than the commercially pure titanium but with the same stiffness and thermal properties. Over 70 % of all alloy grades of Ti-6Al-4V found its uses in aerospace airframe and engine component uses as well as major non-aerospace applications including the marine, offshore and power generation industries. This grade of titanium is an excellent combination of strength, corrosion resistance, weld and fabricability. The speed of scan appreciates with a decrease in dwelling time (Ludovico et al. 2007; Akinlabi et al. 2012), and this factor causes a reduction in powder efficiency during the laser deposition of Ti-6A-l4V (Akinlabi et al. 2012). In other word, the quality of coating can be improved at high scanning speed (Sun and Hao, 2012). Copper has an influence on the microstructure of a composite, causes a change in the graphite phase and enhances the reaction of titanium and carbon (Zhang et al. 2011). LMD process

parameters interaction is a very complex task and difficult to apprehend and so many works have been established on the process parameters influential terminologies (Bontha, 2006; Brandl et al. 2012). (Yasa and Kruth, 2011) worked on laser re-melting on the selective laser melting parts of AISI 316L stainless steel powder and highlighted that almost all the parts with low scan speed and high power, produced higher percentage of porosity and density was improved after laser re-melting. (Thijs et al. 2012) reported on the rate of cooling with varying scanning speed and pointed out a decrease in the size of α- martensitic structure thereby leading to an increase in the Vickers microhardness value and also that a higher scan speed results in some porosity as an implication of unmelted powder region. The risk behind the porosity of weld is not easily quantified which resulted in a loss of premature fatigue failure, increase in service creep, strength of weld and all these properties were attributed to the gas trapped inside the pores and reduces corrosion predominantly (Daugherty and Cannell, 2017]. In the (Science of Loren Pickart for the discovery of copper, accessed 2013), it was found that the risk of copper deficiency is much higher that the excess of copper content in the body. Copper is an excellent conductor of heat and stimulate a warm flow of healing energy. It is an essential metal necessary for many processes in the human body and the deficiency of copper can contribute to a host of health problems such as cancer, impaired brain function, cardiovascular disease, obesity and depression. 2 mg/day was recommended by the Recommended Dietary Intake (RDI) established by the U.S. Food and Drug Administration. The World Health Organization recommended the intake of 10 mg/day of copper as the tolerable upper limit. (Gubler et al. 1953) reported that 50 mg of copper injected into the body of human was completely cleared off within 4 hours. (Harvey et al. 2003) also revealed that due to the efficient mechanism of copper homeostasis, 4-8 mg of copper was taken a day for 1 to 3 months by a volunteer without any adverse effects in the plasma concentration of human body and it was also proved by (Rock at al. 2000) that copper

can improve the anti-oxidant defence in the body. Copper is also known to improve wound healing and brittle bones and the whole body of human contains about 50-120 mg of copper content in which the highest concentration is found in the liver and the brain (Uauy at el. 2008). With all the general applications and functions of copper, no literature has revealed the addition of small amount copper to Ti-6A-l4V for bone implants. (Park et al. 2007) studied the effects of Calcium ion incorporation on bone healing of Ti-6Al-4V alloy implants in rabbit tibiae. The Calcium incorporated in Ti-6Al-4V implants was tested for osteoconductivity after six weeks. Their results revealed that a crystalline $CaTiO_3$ layer was formed on Ti-6Al-4V surfaces implant. (Okazaki et al. 2005) examined the formation of a new bone in rat femur and tibia using various metal implants, 316L stainless steel, Co–Cr–Mo casting alloy, Ti–6Al–4V and Ti–15Zr–4Nb–4Ta alloys. They reported the metal implant to be good markers of osteocompatibility for the investigation of various metal implants. (Reig et al. 2013) investigated the microstructure and mechanical behaviour of pores during Ti–6Al–4V powder sintering. They revealed that in order to improve the behaviour of Ti–6Al–4V for bone application, stiffness must be reduced for the purpose of generating a porous structure. (Zhang et al. 2013) modified the surface of Ti-6Al-4V to enhance bone ingrowth and increase bone formation to create firm osseointegration between the implant and the host bone to minimise the risk of implant losing. (Xiang et al. 2012) fabricated porous Ti-6Al-4V implants using electron beam melting process. Their results on pores showed a size of about 600 μm and a porosity of approximately 57%. Fully porous samples structure coated with bone-like apatite were implanted into cranial defects in rabbits to investigate the in vivo performance. Their results revealed that Ti-6Al-4V implants with well-controlled porous structure, rough surface topography and bone-like apatite layer are beneficial for bone ingrowth.

The motivation for this work is to improve the integrity of Ti-6Al-4V alloy grade 5 with the addition of 1 % of Cu. This alloy has gained advantage in the biomedical implant. Small amount of Cu has been proved of have a good healing property in the body of human. The 1 % of Cu was added to Ti-6Al-4V alloy to improve its confidence in attacking any diseases that comes around the implant.

This research work emphatically ponders on characterising the influence of scanning speed and high powder flow rate on the volume of deposited composites, microstructure, porosity and the microhardness during laser metal deposition of Ti-6Al-4V/Cu composites. The scanning speed was varied for both the Ti-6Al-4V and Cu powders while the laser power and the powder feed rate were kept constant.

2. EXPERIMENTAL SETUP AND PROCEDURES.

The experiment was conducted at the National Laser Centre, Council of Scientific and Industrial Research (NLC-CSIR), Pretoria, South Africa. The equipment used was Ytterbium laser system equipment (YLS-2000-TR), powered at 2000 Watt maximum and connected to a kuka robot with a three way powder jet nozzle attached at its end.

A. MATERIALS AND METHODS

The two powders used were Ti-6Al-4V and Cu powders. The particle sizes of the Ti-6Al-4V and Cu powders varied between 150 and 200 μm. The two powders were fed from two different hoppers. The powders flow through the groove at the base of the hoppers and get sucked into the hose connected to the base of the hoppers and flow to the nozzle end with the help of the carrier gas. An argon gas was supplied to provide a shield during the operation to prevent oxygen contamination on the deposited composite.

A solid plate containing 99.6 % Ti-6Al-4V alloy with a dimension of 102 X 102 X 7.25 mm^3 was used for the substrate. The substrate was sandblasted before deposition in a cubicle containing a shooting gun to remove surface contaminants and to create a rough layer for firm metallographic bonding between the deposit and the substrate. Acetone was used to clean the substrate after sandblasting and dried off with a hand dryer. The powder feeder control of the laser system can be operated at a maximum and minimum flow rate of 10 rev/min and 0.1 rev/min respectively. In this experiment, the powder flow rate (PFR) of Ti-6Al-4V and Cu were maintained at 9.9 rev/min and 0.1 rev/min respectively while the gas flow rate for both powders were maintained at 2.0 l/min throughout the experiment. The process parameters used in this study are shown in the Table I. The beam diameter and track length were maintained at 4 mm and 5 mm respectively. The distance between the nozzle and the substrate distance was kept at 12 mm and the focal length of 210 mm was used throughout the experiment. Five deposits were made on the substrate and labelled samples A to E and the deposited composites were cleaned with metal brush to remove the unmelted powders on them. After the full deposition was made, each sample was sectioned transversely. Each cut samples was mounted in poly fast prior to further characterization processes. The samples were grinded, polished and etched according to E3-11 ASTM International standard guide for preparation of metallographic specimens.

B. VOLUME OF DEPOSITED COMPOSITE.

The volumes of each of the samples from Track 2 of sample B to Track 5 of sample E were calculated using the excel spread sheet with the formulas as shown in equations (i), (ii) and (iii) according to Sloane A133742 . Track 1 of sample A was neglected due to its nature of deposit as shown in Figure 3.

The area of the circular segment of radius [R] is given by:

$$A = R^2 Cos^{-1}\left[\frac{R-h}{R}\right] - [R-h]\frac{W}{2} \ldots\ldots\ldots\ldots\ldots\ldots\ldots\ldots (i)$$

According to Sloane A133742, X = 0.596027. This mathematical expression was not solved analytically but numerically solved.

$$h = 0.596027R \ldots\ldots\ldots\ldots\ldots\ldots\ldots\ldots\ldots\ldots\ldots\ldots\ldots (ii)$$

$$V(L,R,h) = L\left[R^2 Cos^{-1}\left[\frac{R-h}{R}\right] - [R-h]\frac{W}{2}\right] \ldots\ldots\ldots (iii)$$

The abbreviations were designated as follows:

[L] = Deposit length, [W] = Deposit width, [h] = Height of deposit, [R] = Radius of circle, [A] = Area of circular segment and [V] = Volume of deposited composite.

C. MICROSTRUCTURE

The Kroll's reagent was prepared for etching the mounted samples. The etchant was prepared with 100 ml H_2O, 2 ml HF, 4 ml HNO_3. Each sample was etched for 15 seconds, cleaned with ethanol, rinsed under running water and dried off prior to optical observation. Sample A was badly deposited as shown in Figure 3. Samples B to E were only observed under the BX51M Olympus microscope at low and high magnifications each for the macrostructure and the microstructure. The Scanning Electron Microscopy (SEM) analyses were conducted using the TESCAN instrument with Vega TC software to run the analysis.

D. POROSITY EVALUATION

The porosity evaluation was done on the Olympus microscope with stream software. A capture was made on each deposit after the macrostructural observation to evaluate and quantify the percentage of porosity on the sectional surface on the Ti-6Al-4V/Cu deposited composite. The pore analysis was characterized on the deposit leaving alone the substrate. Analysis was done on the pores and the porosity was provided in percentages.

E. HARDNESS TESTS

The microhardness test was also performed on a Vickers hardness machine Zwick/Roell. Hardness was performed on each sample from the top of the deposit to the bottom thereby making eight indentations on the laterally sectioned surface of the deposited composite to the substrate. A load of 500 g and a dwell time of 15 seconds were used throughout the hardness test according E384 ASTM standard.

3. RESULTS AND DISCUSSION

A. Physical observation of the deposited tracks

Due to the defect on track 1, it was not characterised further. From Table II, it was found that the height and the width of the deposited composites decreased with an increase in scanning speed. The very low scanning speed and high powder caused the badly deposited composite. The material efficiency was very low with the scanning speed used. This was in agreement with (Akinlabi et al. 2012). Table II presents the sample tracks and the physical measurements for the length of deposit, the deposit width, deposit height, as well as the radius of circle, the area of circular segment and the volume of deposited composite which were solved using the equations (i), (ii) and (iii) and are provided in tabular form.

B. Volume and area of the deposited tracks

The volume of the composite shows a greater decrease as the scanning speed decreases as shown from sample B to E. The area of segment was calculated using equation (1). The value of $x = 0.596027$ is constant which gives the ratio of the height to the radius of circle of deposited track. The volume of the deposited track obtained strongly depends on the PFR used. The mass of a particular composite can be determined with the volume calculated and

once the density of the deposited material is known. This volume calculated will reduce the use of weigh balance to measure the mass of material deposit.

C. Microstructural Evaluation

Both the macrostructure and microstructure were taken into consideration during the optical microstructural analysis. The deposit of sample B as shown in Figure 5(a) was invariably on the substrate creating some pores at the interface and extended almost to the middle of the deposit. A low metallographic bonding was observed due to the fact that the melt pool that was created on the substrate for the bonding was low. More powders were deposited on the melt pool with a total PFR of 10 rev/min for both powders since the scanning speed is low. The height of the deposit was high and shortened as the scanning speed increases. The heat input required to melt the powders was not enough and the height observed was due to the high PFR of the Ti-6Al-4V powder used at a low scanning speed of 0.06 m/min. The macrostructures at the top of the cross section of samples B to E are coarser than the mid area of the cross section which could be as a result of thermal gradient and this was in agreement with (Puebla et al. 2012). Figure 6(b) shows a reduced height of the deposit compared to the sample B in Figure 6(a). Some unmelted powders was observed from the macrographs of samples C, D and E as shown in Figures 6(b) to 6(d) owing to the low heat input and the time shortage of scan speed increment. Figures 6(c) and 6(d) show some bonding at the interface between the composite and the fusion zone (FZ). The little fusion that was observed occur as a result of the increase in the scanning speed over the laser power of 1000 W used. Figure 7(a) shows the microstructure of sample B at 10 X magnificaton. Macroscopic banding or layering was observed at the middle of the deposited composite and decreases when the scanning speed reduces. Figure 7(b) shows the composite, fusion zone (FZ) and the heat affected zone (HAZ). The crystals of the deposit has a little epitaxial growth towards the FZ.

Acicular microstructure was found in all the samples from B to E and decreases as the scanning speed increases. Due to 1% of Cu added to Ti-6Al-4V powder in this experiment, the structure of Cu was not observed in the microstructures but intermetallics set in. Figure 7(c) shows the widmanstätten structure and α-colony under the SEM observation. A coarse widmanstätten structure was formed as a result of fast cooling rate of the deposited composite. These widmanstätten structures were formed by a mechanism of martensitic decomposition to phases and grain coarsening during LMD, and recrystallization was significantly not pronounced.

D. Porosity Characterization

Figure 8 shows the histogram of the percentage porosity, porosity distribution and the average value of the pores. The histogram was plotted for sample track B to sample track E as shown in Figure 8. An indication shows that an increase in scanning speed changes the orientations of the pores generated. The variations in the laser scan speed could facilitate a degree of control over morphology of the porosity formed (Savalani et al. 2007). The mean value for sample D and E are approximately 30 μm. In general application, a pore size of 5 to 10 μm enables the in growth of fibrous tissue and pore sizes ranging between 20 and 60 μm are good for cell spreading and proliferation (Hao et al. 2004; Hollister et al. 2002). The percentage of porosity increases by 4.5 % from sample B to sample C and this could be due to the unmelted powder as observed in sample C and more gas are entrapped in between two or more particles thereby show some wider pores in sample C than sample B. Sample D and sample E show a drastic reduction in the percentage porosity and pore size distribution. The reason been that the scanning speed was fast with the laser power used and the volume of deposition was small and could accommodate enough gas entrapment.

E. Microhardness

The microhardness of Ti6Al4V/Cu deposited composite shows an increase the hardness value as the scanning speed increases, this is in agreement with (Brandl et al. 2012) and at the same time the rate of reduction percentage porosity also influences the hardness value. An indication shows that the percentage of hardness increase between the substrate and each samples from B to E as indicated on the histogram is between 10 % and 16 % approximately.

4. CONCLUSIONS

Ti-6Al-4V/Cu powder was successfully deposited on Ti-6Al-4V substrate and characterized. The volume of the deposited track obtained strongly depends on the PFR used and the rate at which the scanning speed was introduced. The highest percentage of porosity was observed in sample C with a scanning speed of 0.9 m/min due to the higher PFR and low scanning speed at a constant power of 1000 W. The evolving microstructures show a layer of macroscopic banding in a single layer of track deposit and α-phase acicular microstructure which decreases in size and thickness as the scanning speed is increased. The strength of Ti-6Al-4V/Cu powder deposit was improved as compared to the parent material of Ti-6Al-4V substrate. The porosity obtained between samples D and E can be used for cell spreading and proliferation.

Further research work is required to immerse the samples in Hank's balanced salt solution with the combination of blood serum and tissue extract for some weeks in order to critically observed and analyse the reaction of laser deposited Ti-6Al-4V/Cu composites in the solution.

Acknowledgments

This work is supported by the Council of Scientific and Industrial Research (CSIR), National Laser Centre, Rental Pool Programme, Pretoria, South Africa and also for the award of the Africa Laser Centre bursary to the main author.

REFERENCES

Akinlabi ET, Mahamood RM, Shukla M, Pityana S (2012). Effect of Scanning Speed on Material Efficiency of Laser Metal Deposited Ti6Al4V. World Academy of Science, Engineering and Technology 71: 1531-1535.

Bontha S, (2006). The Effect of Process Variables on Microstructure in Laser-Deposited Material. PhD Thesis, Wright State University, Engineering.

Brandl E, Schoberth A, Leyens C (2012). Morphology, microstructure, and hardness of titanium (Ti-6Al-4V) blocks deposited by wire-feed additive layer manufacturing (ALM). Materials Science and Engineering. 532: 295-307.

Calculator for Conversion between Vickers Hardness Number and SI Units MPa and GPa. http://www.gordonengland.co.uk/hardness/hvconv.htm. Surface Engineering Forum. Accessed 2014.

Compare Materials. Commercially Pure Titanium and 6Al-4V (Grade 5) Titanium" (http://www.makeitfrom.com/compare/?left=CP_Titanium& right=Titanium_Grade_5) Accessed 2014.

Daugherty WL, Cannell GR (2003). Analysis of porosity associated with Hanford 3013 outer container welds. Practical Failure Analysis. 3: 56-62.

E3-11 Standard Guide for Preparation of Metallographic Specimens, ASTM International.

Gubler CJ, Lahey ME, Cartwright GE, and Wintrobe MM (1953). Studies on copper metabolism. IX. The transportation of copper in blood. Journal of Clinical Investigation. 32: 405-414.

Hao L, Lawrence J, Chian KS (2004). The effect CO_2 laser irradiation on the surface properties of a magnesia partially stabilised zirconia (MgO-PSZ) bioceramic and the subsequent improvements in human osteoblast cell adhesion. Journal on Biomaterial Application. 19: 81-105.

Harvey LJ, Majsak-Newman G, Dainty JR, Lewis DJ, Langford NJ, Crews HM, Fairweather-Tait SJ (2003). Adaptive responses in men fed low- and high-copper diets. British Journal of Nutrition. 90: 161-168.

Hollister SJ, Maddox RD, Taboas JM (2002). Optical design and fabrication of scaffolds to mimic tissue properties and satisfy biological constraints. Biomaterials. 23: 4095-4103.

Ludovico DA, Angelastro A, Campanelli SL (2007). Experimental Analysis of the Direct Laser Metal Deposition Process", Polytechnic of Bari, Department of Management and Mechanical Engineering. Italy. www.intechopen.com. 253-273.

Lutjering G, Williams JC, (2007). Titanium-Springer, Engineering Materials and processes. 12: 1-442.

Moiseyev VN (2006). Titanium alloys: Russian aircraft and aerospace applications. CRC Press Taylor & Francis Group. 2: 169-180.

Okazaki Y, Gotoh E, Nishimori M, Katsuda S, Manabe T, Kobayashi K (2005). Osteocompatibility of Stainless Steel, Co–Cr–Mo, Ti–6Al–4V and Ti–15Zr–4Nb–4Ta Alloy Implants in Rat Bone Tissue. Materials Transactions. 46: 1610-1617.

Puebla K, Murr LE, Gaytan SM, Martinez E, Medina F, Wicker RB (2012). Effect of Melt Scan Rate on Microstructure and Macrostructure for Electron Beam Melting of Ti-6Al-4V. Materials Sciences and Applications. 3: 259-264.

Reig L, Toja C, Busquets DJ, Amigó V (2013). Microstructure and Mechanical Behavior of Porous Ti–6Al–4V Processed by Spherical Powder Sintering. Materials. 6: 4868-4878.

Rock E, Mazur A, O'Connor JM, Bonham MP, Rayssiguier Y, Strain JJ (2000). The effect of copper supplementation on red blood cell oxidizability and plasma antioxidants in middle-aged healthy volunteers. Free Radical Biology and Medicine. 28: 324-329.

Savalani MM, Hao L, Zhang Y, Tanner KE, Harris RA (2007). Fabrication of porous bioactive structures using the selective laser sintering technique. Part H: Journal on Engineering in Medicine. 221: 876-886

Sloane NJA. The on-line Encyclopedia of Integer Sequences" http://mathworld.wolfram.com/quarter-tankproblem.html.Sequence A133742. Accessed 2013.

Sun Y, Hao M (2012). Statistical analysis and optimization of process parameters in Ti6Al4V laser cladding using Nd:YAG laser, Optics and Lasers in Engineering. 50: 985–995.

The science of Loren Pickart PhD, True Science, Anti-aging. The essentials of copper. Your Body's Protective and Anti-Aging Metal. Accessed 2014.

Thijs L, Verhaeghe F, Craeghs T, Van Humbeeck J, Kruth JP (2010). A Study of the Microstructural Evolution during Selective Laser Melting of Ti-6Al-4V. Acta Materialia. 58: 3303-3312.

Uauy R, Maass A, Araya M (2008). Estimating risk from copper excess in human populations". American Journal of Clinical Nutrition (suppl): Printed in USA. © 2008 American Society for Nutrition. 88: 867S-871S.

Wohlers T (2011). Wohlers Report 2011: Additive Manufacturing and 3D Printing, State of the Industry. Ft. Collins, CO: Wohlers Associates.

Woo Park J, Bum Park K, Young Suh J (2007). Effects of calcium ion incorporation on bone healing of Ti6Al4V alloy implants in rabbit tibiae. Biomaterials. 28: 3306–3313.

Xiang L, Yun L, Chengtao W, Wenguang Z, Yuanchao L (2012). Fabrication and in vivo evaluation of Ti6Al4V implants with controlled porous structure and complex shape, Frontiers of Mechanical Engineering. 7: 66-71.

Yasa E, Kruth J (2011). Application of Laser Re-melting on Selective Laser melting parts. APEM JOURNAL, Advances in production Engineering and Management. 64: 259-270.

Zhang X, Zheng G, Wang J, Zhang Y, Zhang G, Li Z, Wang Y (2013). Porous Ti6Al4V Scaffold Directly Fabricated by Sintering. Preparation and *In Vivo* Experiment, Hindawi Publishing Corporation Journal of Nanomaterials. Volume 2013, Article ID 205076, 7 pages.

Table I: EXPERIMENT PROCESS PARAMETERS

Sample Designation	Laser Power (W)	Scanning Speed (m/min)	Powder Feed Rate [Ti-6Al-4V] (rev/min)	Powder Feed Rate [Cu] (rev/min)	Gas Flow Rate [Ti-6Al-4V] (l/min)	Gas Flow Rate [Cu] (l/min)
A	1000	0.06	9.9	0.1	2.0	2.0
B	1000	0.3	9.9	0.1	2.0	2.0
C	1000	0.6	9.9	0.1	2.0	2.0
D	1000	0.9	9.9	0.1	2.0	2.0
E	1000	1.2	9.9	0.1	2.0	2.0

Legend

Table I shows the process parameters used for this study. The samples were named from A to E. Throughout the experiment, a constant laser power of 1000W was used while the scanning speeds were varied between 0.06 m/min and 1.2 m/min. Due to the 1 % of Cu involved, a very high powder flow rate was used.

Table II: MEASUREMENTS OF THE LENGTH, WIDTH AND HEIGHT OF THE DEPOSITED Ti6Al4V/Cu COMPOSITES

Sample Tracks	[L] (mm)	[W] (mm)	[h] (mm)	[R] (mm)	[R-h] (mm)	[A] (mm^2)	[V] (mm^3)
Track 2	50	3.36	2.43	1.80	-0.63	7.29	291.80
Track 3	50	3.19	1.4	1.61	0.21	3.40	135.81
Track 4	50	2.93	0.81	1.73	0.92	1.68	67.00
Track 5	50	2.82	0.67	1.82	1.15	1.31	52.59

Legend

Table II depicts the physical measurement of the deposited composites from Track 2 to Track 5. Track 1 was neglected due the poor deposition. The speed of 0.06 m/min used for Track 1 was too low with the high powder flow rate applied. The dimensions were carried out in other to calculate the area of circular segment and the volume of deposited composite. With the values of the volume obtained, the mass of the each deposit can be known. This phenomenon tends to reduce the use of weigh to measure each mass of the deposited composite.

LISTS OF FIGURES

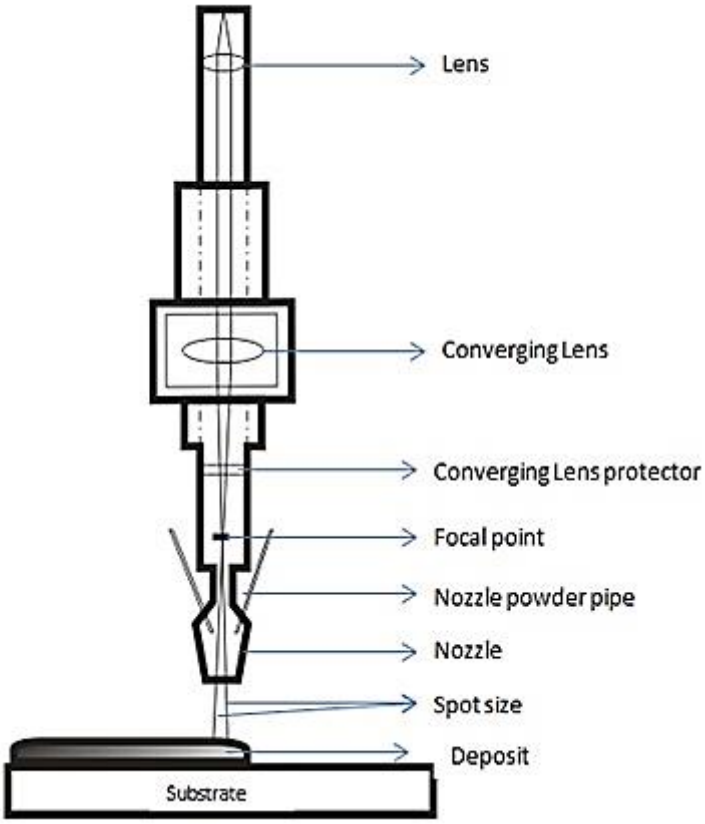

Figure 1

Figure 1 shows a typical 2D view of the nozzle attached to the kuka robot. The nozzle is connected to a cylindrical component which embedded a glass of 2 mm thickness. The glass serves as a protector for the converging lens when the laser melts the powder. The rate of divergence at the focal point determines the spot size. The laser passes through the middle of the nozzle while the powders flows through the three way hole at the tip of the nozzle. The three way holes are at 120^{o} to each other.

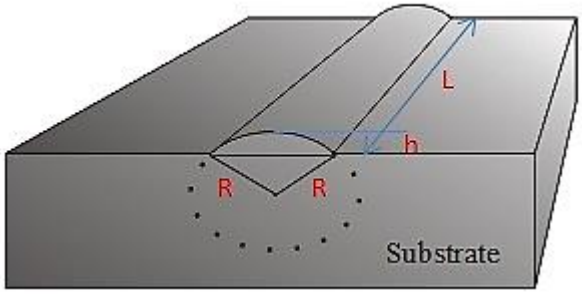

Figure 2

The schematic view of the deposited composite was shown in Figure 2. The view is a sample image of the composite as deposited on the substrate. The geometry for calculating the volume of the deposited composite was indicated in Figure 2. Since the height, width and length of deposit has been developed, the values were substituted into the Sloane's formular to achieve the volume of the deposited composite.

Figure 3

Figure 3 presents the deposited tracks of Ti-6Al-4V/Cu composite on the Ti-6Al-4V substrate. A close observation of the deposited tracks shows that track 1 depicts a badly deposited track at a scanning speed of 0.06 m/min. It was in folded form and the deposit was

only formed on the substrate that is, there was no penetration between the deposited composite and the substrate. Other tracks from sample track B to E show a good deposit on the substrate.

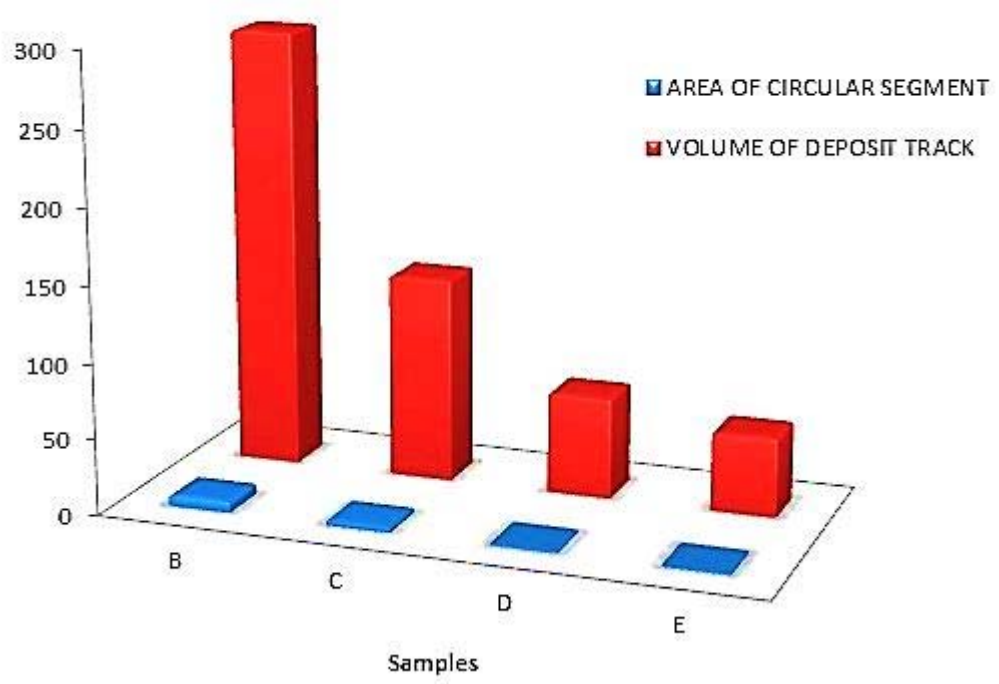

Figure 4

The volume of deposited composites and area of circular segment of the deposit were plotted in the histogram for all the samples from except sample A as shown in Figure 4.

The area of segment decreases slightly as the scanning speed increases. The histogram shows a stepwise structure as the volume decrease with respect to the increment in scanning speed. In other word, the volume of the deposited composite is directly proportional to the scanning speed and irrespective of the powder flow rate or gas flow rate used.

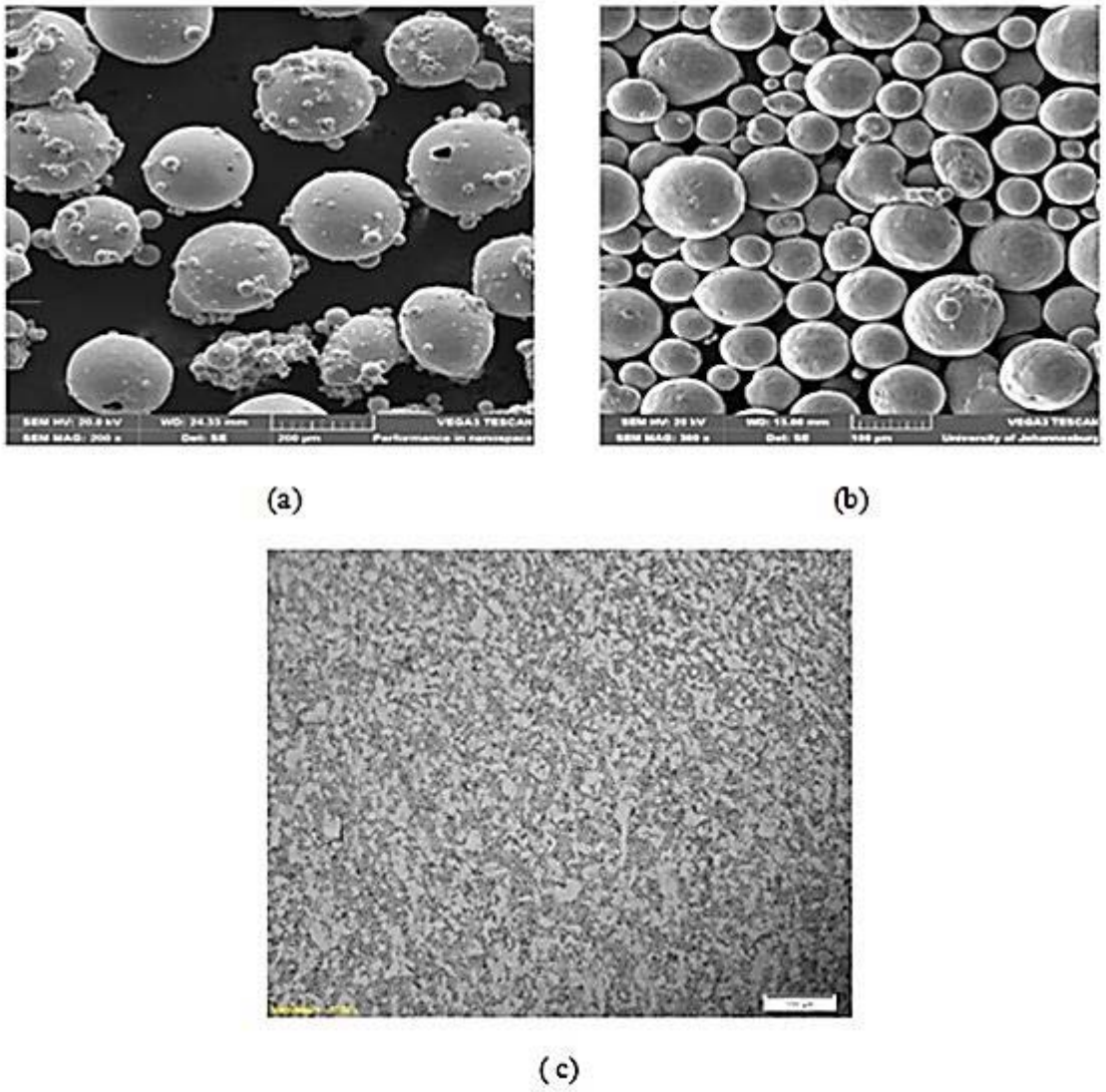

Figure 5

Figures 5(a) and 5(b) show the SEM morphology of the Ti-6Al-4V and Cu powders. Both powders were observed to be spherical in shape with different particle sizes. Figure 5(c) shows the microstructure of the cross section of the substrate. Two phases were observed in the microstructure of the substrate, the α-dark phase and the β-light phase.

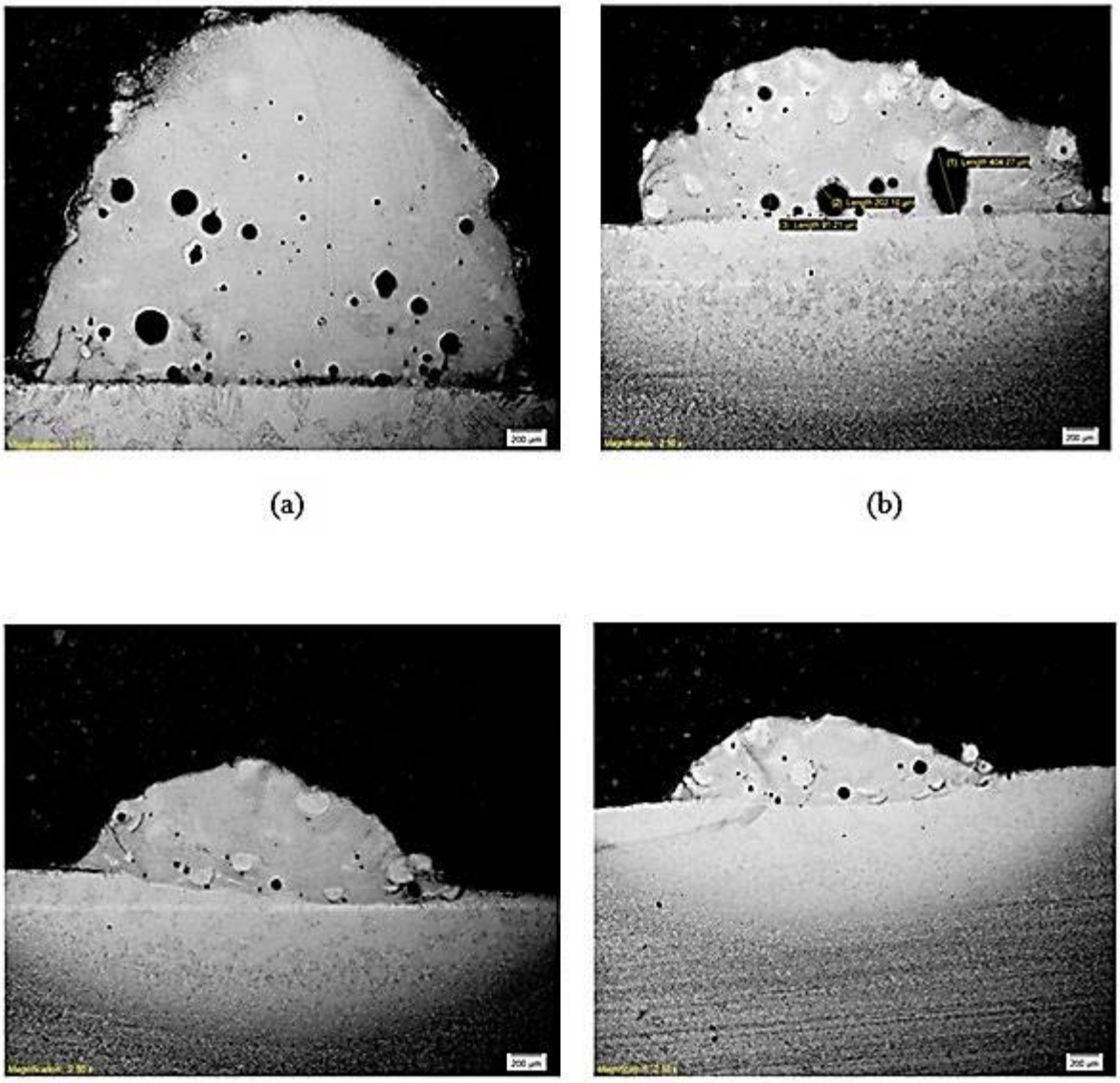

Figure 6

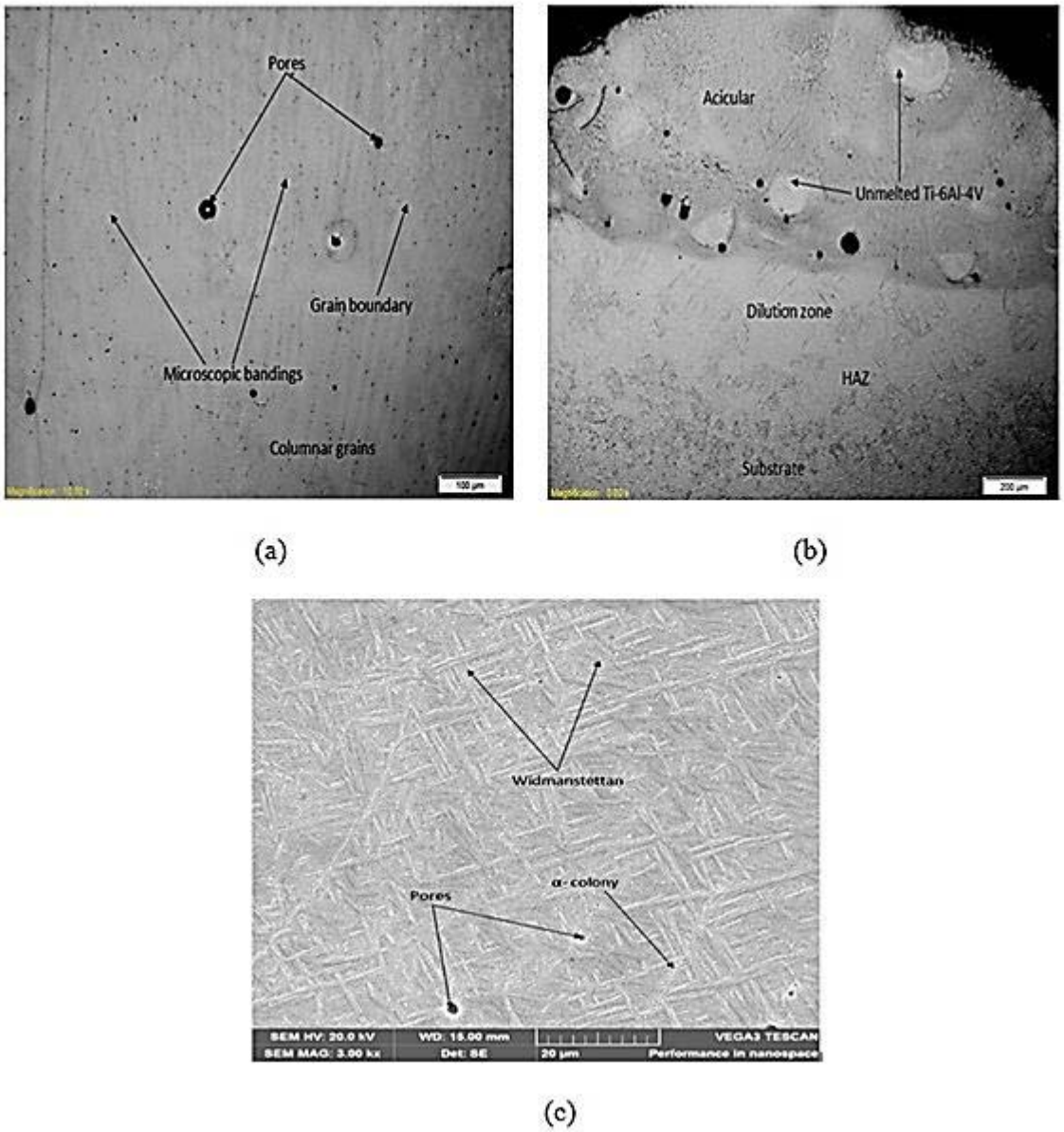
Pores
Grain boundary
Microscopic bandings
Columnar grains
(a)
Acicular
Unmelted Ti-6Al-4V
Dilution zone
HAZ
Substrate
(b)
Widmanstettan
α-colony
Pores
SEM HV: 20.0 kV
WD: 15.00 mm
VEGA3 TESCAN
SEM MAG: 3.00 kx
Det: SE
20 µm
Performance in nanospace
(c)

Figure 7

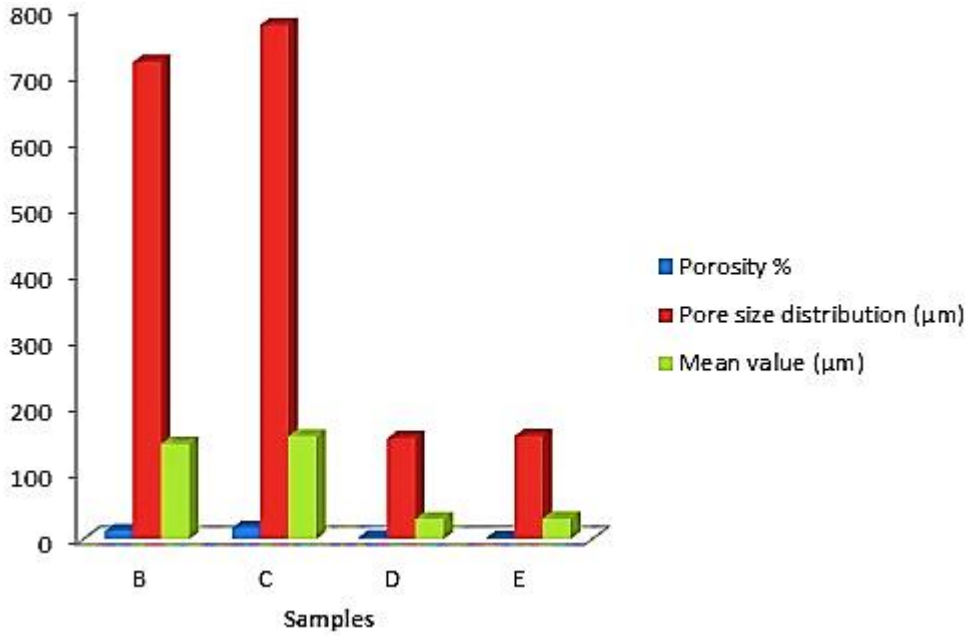

Figure 8

Figure 8 shows the histogram of the percentage porosity, the pore size distribution and the mean values against the samples. The histogram indicates that the rate of porosity decreases as scanning speed increases.

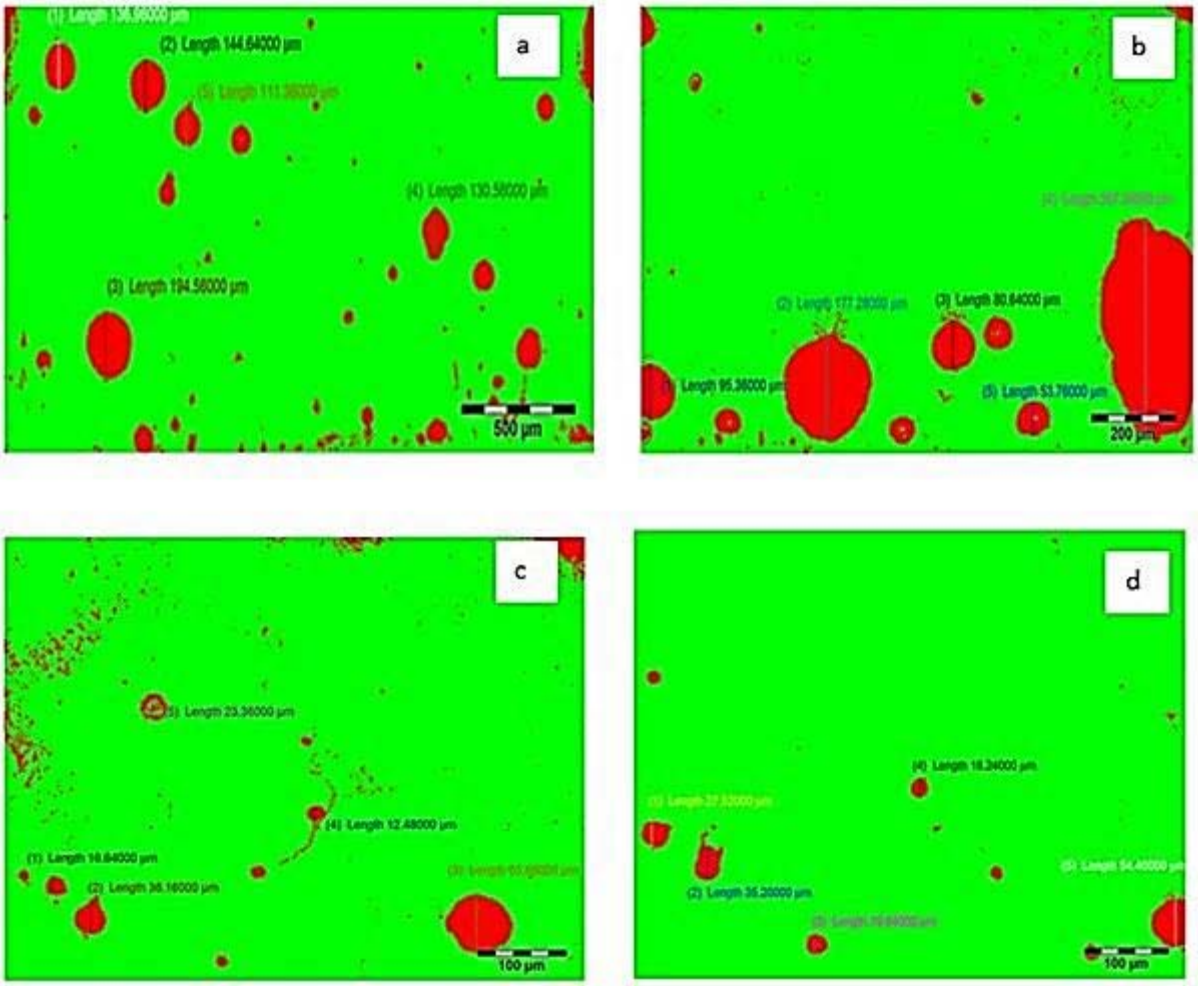

Figure 9

Figure 9 shows the phase analysis of porosity for sample B to sample E. The green colour observed is the cross section of the Ti-6Al-4V/Cu composite. The red colours showed on the composite are the pores. The pore size distribution was measured as a result of wideness of the pores in each sample.

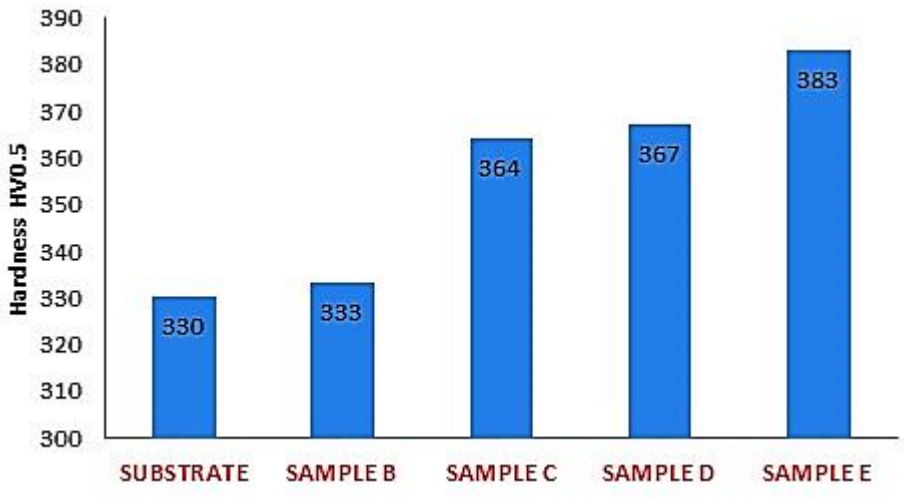

Figure 10

The average Vickers microhardnes of the samples are presented in Figure 10. Samples B, C, D and E possess the hardness of 3.27 GPa, 3.57 GPa, 3.60 GPa and 3.76 GPa respectively. The values were calculated according to the conversion factor of hardness. In other words, the hardness of the composite samples increases as the scanning speed increases.